A REALISTIC LARGE-SIGNAL MESFET MODEL FOR SPICE

Anthony E Parker

Electronics Department, Macquarie University
Sydney, 2109, Australia – tonyp@mpce.mq.edu.au

ABSTRACT

A large-signal MESFET model, implemented with new techniques, has continuity and rate dependence. These features provide accurate prediction of circuit gain and distortion. The techniques also improve simulation speed. The model has improved descriptions of capacitance and bias dependence. It has small-signal S-parameter accuracy extended to a wide range of operating conditions. This model is now in several simulators including Pspice v6.2.

INTRODUCTION

This paper describes a comprehensive MESFET model. It is a realistic description of measured characteristics over all operating regions. It describes sub-threshold conduction and breakdown. It has frequency dispersion of both transconductance and drain conductance, and derates with power dissipation. All derivatives are continuous for a realistic description of circuit distortion and intermodulation.

The new model is a valuable tool for the design of modern communications circuits. A single characterisation is valid for various operating modes encountered in microwave circuits. Descriptions of the controlled-resistance and controlled-current regions use independent power-laws. Its rate dependence adapts the model to any bias condition. There is no requirement for a suite of model parameters.

Transconductance and drain conductance dispersion occur during high frequency excursions around the bias point. This gives correct small-signal S-parameters in any bias region including the controlled-resistance region. A thermal time constant controls response to power dissipation. The rate dependent descriptions can simulate looping observed in curve tracer measurements.

The model describes complex behaviour in greatly reduced simulation time. A nested transformation scheme ensures high-order continuity. This gives substantially improved convergence time. State variables improve speed of rate dependence simulation by eliminating extra circuit nodes.

The following section presents the model's description of dc drain-source current. The subsequent section gives details of rate dependence and frequency dispersion. Finally, this paper presents the charge storage model.

INTRINSIC CURRENT MODEL

Intrinsic drain-source current is central to the model. Gate charge is described by an improved version of the model proposed by Statz *et al.*[1]. Extrinsic gate-source and gate-drain diodes describe the gate junction. Source and drain contact resistances are considered extrinsic elements.

A general power-law function of effective gate and drain potentials, V_{gt} and V_{dt}, describes the intrinsic drain-source current. Parameters β and Q control the model.

$$I_d = \beta \cdot V_{gt}^{Q} \cdot \left[1-\left(1-V_{dt}/V_{gt}\right)^{Q}\right] \qquad (1)$$

This is the base equation for the model. A *nested* series of *transformations* of the external terminal potentials modify its arguments. This adds short-channel behaviour to the model incrementally.

The model describes early saturation of a MESFET by placing a restriction on the maximum value of V_{dt}. Setting the restriction to V_{gt} would describe simple pinch-off saturation. The model selects the lesser of V_{gt} and an earlier saturation potential. The latter is set by parameter ξ and the channel depletion potential, $W_{oo} = \phi_b - V_{TO}$. A smooth function selects the required drain-source saturation

TH 3F

0-7803-3246-6/96/$5.00 © IEEE

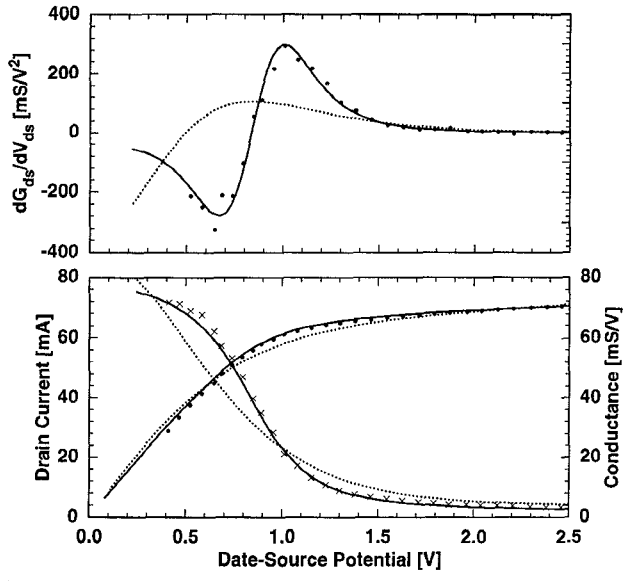

Figure 1: Current saturation and its first and second derivatives described by the new model ——, and a hyperbolic tangent ·····. Measured data (•, ×) is also shown.

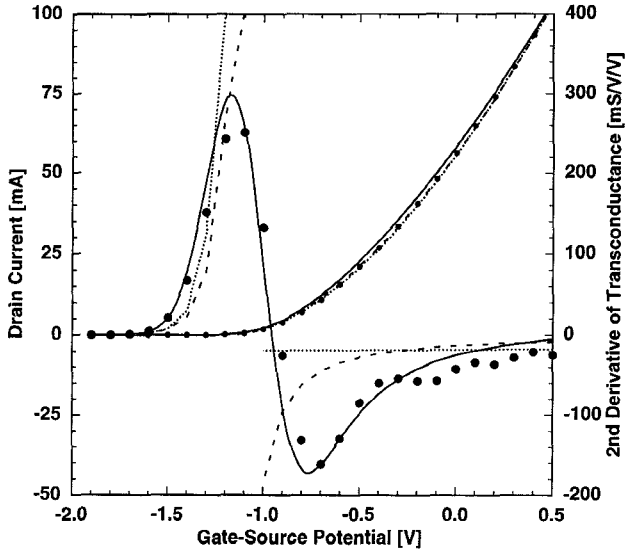

Figure 2: Saturated drain current and its third derivative described by three different models: ····· Statz *et al.* [1] and - - - McCamant *et al.* [8] with exponential subthreshold regions, and —— the new model. Measured data, •, is also shown.

potential, V_{sat}.

$$V_{sat} = \frac{V_{gt} \cdot \xi \cdot W_{oo}}{V_{gt} + \xi \cdot W_{oo}} \tag{2}$$

A smooth transformation implements the restriction of V_{dt}. Parameter z controls the shape of the saturation knee.

$$V_{dt} = \tfrac{1}{2}\sqrt{\left(V_{dp} \cdot \sqrt{1+z} + V_{sat}\right)^2 + z \cdot V_{sat}^2} - \tfrac{1}{2}\sqrt{\left(V_{dp} \cdot \sqrt{1+z} - V_{sat}\right)^2 + z \cdot V_{sat}^2} \tag{3}$$

This provides a description of transition to saturation that correctly describes drain-source conductance. Figure 1 shows the improvement over the hyperbolic tangent function used in several other models [2].

The model also gives independent control over the controlled-current and controlled-resistance regions [3]. It obeys a P, rather than Q, power-law in the region near zero V_{ds}. A transformation of the applied drain-source potential implements the *dual (P-Q) power-law*.

$$V_{dp} = V_{ds} \cdot \frac{P}{Q}\left(\frac{V_{gt}}{W_{oo}}\right)^{P-Q} \tag{4}$$

A single set of dual power-law model parameters can describe both the controlled-resistance and controlled-current regions.

Description of sub-threshold conduction is a transformation of the gate-source potential. This gives an exponential approach to the gate-source pinch-off potential.

$$V_{gt} = V_{ST}\left(1 + M_{VST} V_{ds}\right) \cdot \ln\left(1 + \exp\left(\frac{V_{gst}}{V_{ST}\left(1 + M_{VST} V_{ds}\right)}\right)\right) \tag{5}$$

The terms M_{VST} and V_{ST} are model parameters, and V_{gst} is gate-source potential relative to the channel's pinch-off potential. The pinch-off potential includes frequency dispersion terms described in the next section.

This transformation, like the others in the model, is well behaved and infinitely differentiable. Derivatives of the model remain continuous. Figure 2 shows the resulting third-order derivative. It is a superior description of measurement that can realistically describe intermodulation distortion [3]. Figure 3 shows simulated and measured harmonic distortion of a typical MESFET. The simulated results represent the general structure of the harmonic spectrum well.

FREQUENCY DISPERSION

At high frequencies the model's output conductance increases by a factor γ_{hf}/γ_{lf} and its transconductance reduces by a factor $(1-\gamma_{hf}-\eta_{hf})/(1-\gamma_{lf})$. Separation of these dispersive effects provides much better simulation of small-

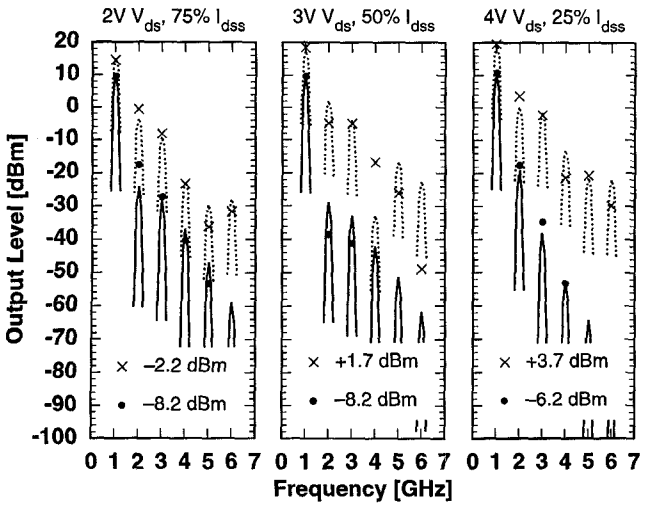

Figure 3: Measured (×, •) and simulated (lines) harmonic distortion of a 900×1 μm MESFET operating in common-source configuration with 50Ω source and load impedances. Results are for two input power levels.

signal behaviour. Modulation of the pinch-off potential by average gate-drain and gate-source *feedback* potentials performs the dispersion.

$$V_{gst} = V_{gs} - V_{TO} - \gamma_{lf} \cdot \overline{V_{gd}} - \gamma_{hf} \cdot \left(V_{gd} - \overline{V_{gd}}\right) - \eta_{hf} \cdot \left(V_{gs} - \overline{V_{gs}}\right) \tag{6}$$

Averages are calculated over a user defined time constant, τ_G, which would normally be between 0.1 and 1 ms. The SPICE implementation uses state variables in a finite difference calculation of the averages using equation (7).

$$\overline{x} = x - \tau_G \cdot \frac{d}{dt}\overline{x} \tag{7}$$

The model adjusts the high-frequency dispersion with bias. The parameters in (6) are varied with average bias by nine model parameters (*LFGAM* to *HFE2*).

$$\begin{aligned} \gamma_{lf} &= LFGAM - LFG1 \cdot \overline{V_{gs}} - LFG2 \cdot \overline{V_{gd}} \\ \gamma_{hf} &= HFGAM - HFG1 \cdot \overline{V_{gs}} - HFG2 \cdot \overline{V_{gd}} \\ \eta_{hf} &= HFETA + HFE1 \cdot \overline{V_{gd}} + HFE2 \cdot \overline{V_{gs}} \end{aligned} \tag{8}$$

This provides a much better simulation of S-parameters.

Two feedback potentials provide a significant improvement over models that use the average drain-source potential [4],[5],[6]. The new model can simulate the characteristic complexity observed in a curve tracer measurement [7]. Figure 4 shows an example of this.

Drain current is scaled with power dissipation. This correction for junction heating is based on [8].

$$I_{ds} = \frac{I_d}{1 + \delta \cdot \overline{V_{ds} I_d}} \tag{9}$$

The term δ is a model parameter. Note that the model calculates average dissipated power rather than use instantaneous power. The calculation is over a time constant, τ_D, using the algorithm of equation (7).

The thermal time constant is a realistic feature omitted from many models. This omission in these models tends to balance their lack of transconductance dispersion. The two feedback potentials in the new model allow it to separate the dispersion and heating effects correctly. This provides a much better simulation of small-signal operation.

CHARGE STORAGE MODEL

The model uses an enhanced charge storage description based on that of Statz *et al.* [1]. This is controlled by model parameters C_{GS} and C_{GD}. The total gate charge, Q_{gg}, is given by

$$Q_{gg} = 2C_{GS}\phi_b \left(1 - \sqrt{1 - V_{new}/\phi_b}\right) + C_{GD} V_{eff2}. \tag{10}$$

A new parameter adds gate-source fringing capacitance to the effective gate-source potential calculation. Capacitance is reduced by factor X_C, rather than to zero, when the device is pinched-off.

$$V_{new} = V_{eff1} X_C + \tfrac{1}{2}(1 - X_C)\left(\left(V_{eff1} + V_{TO}\right) + \sqrt{\left(V_{eff1} - V_{TO}\right)^2 + \left(0.2/(1 - X_C)\right)^2}\right) \tag{11}$$

Parameter γ_{AC} modulates the effective depletion potentials.

$$\begin{aligned} V_{eff1} &= \tfrac{1}{2}\left(V_{gs} + V_{gd} + \sqrt{V_{ds}^2 + \alpha^2}\right) + \gamma_{AC} V_{ds} \\ V_{eff2} &= \tfrac{1}{2}\left(V_{gs} + V_{gd} - \sqrt{V_{ds}^2 + \alpha^2}\right) + \gamma_{AC} V_{ds} \end{aligned} \tag{12}$$

where

$$\alpha = \frac{\xi}{\xi + 1} \cdot \frac{\phi_b - V_{TO}}{2} \tag{13}$$

This simple addition introduces bias dependence to the capacitance model, which improves its fit to measured junction capacitances.

Control over forward-bias junction capacitance is also provided with the parameter F_C. When $V_{new} > F_C \phi_b$ the

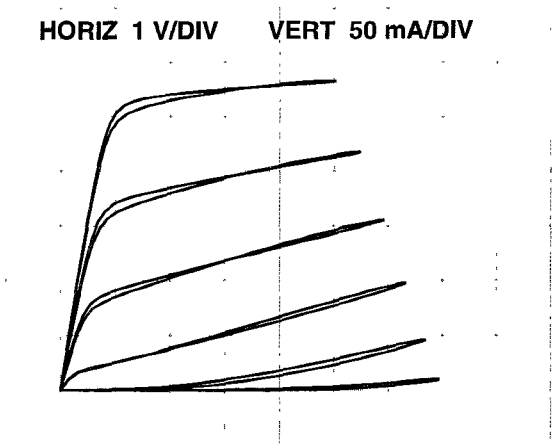

Figure 4: Simulated curve tracer display for a typical MESFET. The shape requires both source-gate and drain-gate feedbacks.

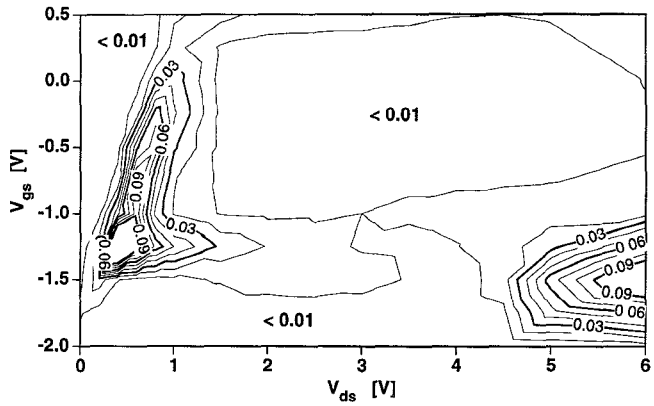

Figure 5: Error in simulated S-parameters of a MESFET's referenced to measurements at 2 GHz. Pinch-off is at –1.5 V. The error function is the sum of squares of differences between simulation and measurement, $\sum |S_{ij}^m - S_{ij}^s|^2$.

gate charge is given by

$$Q_{gg} = C_{GS}\phi_b \left\{ 2\left(1-\sqrt{1-F_C}\right) + \frac{(V_{new}/\phi_b - F_C)^2}{4(1-F_C)^{3/2}} + \frac{(V_{new}/\phi_b - F_C)}{(1-F_C)^{1/2}} \right\} + C_{GD} V_{eff2} \quad (14)$$

Overall small-signal performance of the model is illustrated in figure 5. This shows the accuracy of predicted S-parameters over a wide range of bias conditions. Note that simulation is accurate at V_{ds} = 0 and in the subthreshold region. The error near the saturation knee of the device is a consequence of sensitivity to the rapid changes in S_{22}, rather than increased error in the model.

CONVERGENCE

Despite the model's sophistication, it runs up to five times faster than simpler descriptions that do not use the nested transformation scheme. The improvement is due to the overall continuity of the model, which permits rapid convergence. Also, average potentials are accumulated in state variables rather than extra nodes in the simulator [9].

CONCLUSION

The comprehensive MESFET model presented here is accurate over an extended range of operating conditions. It features high-order continuity for realistic prediction of intermodulation and improved convergence speed. The model has sufficient detail to predict high frequency S-parameters over all bias points. The model has been implemented in various industry standard simulators including those by UC Berkeley (SPICE 3f4), EEsof, MicroSim, Anacad, and Intusoft (Source code is at ftp://ftp.mpce.mq.edu.au/pub/elec/spice/patches/jfet2/ for the SPICE3F4 implementation).

ACKNOWLEDGMENTS

This work is funded by Macquarie University, the Australian Telecommunications and Electronics Research Board, and the Australian Research Council. The author wishes to thank Mike Murphy and Mike Heimlich at M/A-COM, Lowell, MA for their assistance with this work.

REFERENCES

(1) H. Statz, P. Newman, W. Smith, R. A. Pucel and H. A. Haus, "GaAs FET device and circuit simulation in SPICE," *IEEE Transactions on Electron Devices*, vol. 34, no. 2, pp. 160-169, February 1987.

(2) W. R. Curtice, "GaAs MESFET modeling and nonlinear CAD," *IEEE Transactions on Microwave Theory and Techniques*, vol. 36, no. 2, pp. 220-230, February 1988.

(3) A E. Parker and D. J. Skellern, "Improved MESFET characterisation for analog circuit design and analysis," *1992 IEEE GaAs IC Symposium*, pp. 225-228, Miami Beach, October 4-7, 1992.

(4) C. Camacho-Peñalosa and C. S. Aitchison, "Modelling frequency dependence of output impedance of a microwave MESFET at low frequencies," *Elec Lett*, vol. 21, no. 12, pp. 528-529, 6th June 1985.

(5) N. Scheinberg, R. J. Bayruns and R. Goyal, "A low-frequency GaAs MESFET circuit model," *IEEE Journal of Solid-State Circuits*, vol. 23, no. 2, pp. 605-608, April 1988.

(6) J. M. Golio, M. G. Miller, G. N. Maracas and D. A. Johnson, "Frequency-dependent electrical characteristics of GaAs MESFET's," *IEEE Elec Dev*, vol. 37, no. 5, pp 1217-1226, May 1990.

(7) P. H. Ladbrooke and S. R. Blight, "Low-field low-frequency dispersion of transconductance in GaAs MESFET's," *Tran Elec Dev*, vol. 35, no. 3, pp. 257-267, March 1988.

(8) A. J. McCamant, G. D. McCormack and D. H. Smith, "An improved GaAs MESFET model for SPICE," *IEEE Transactions on Microwave Theory and Techniques*, vol. 38, no. 6, pp. 822-824, June 1990.

(9) A. E. Parker, "Implementing SPICE models with high-order continuity and rate dependence," *IEE Proceedings on Circuits, Devices and Systems*, vol. 141, no. 4, pp. 251-257, August 1994.